Effect of nonlinear tide-surge interaction in the Pearl River Estuary during Typhoon Nida (2016)

Linxu Huang[1,2], Tianyu Zhang[2,3,4], Shouwen Zhang[2,6*], Hui Wang[1,5]

1. Institute of Marine Science and Technology, Shandong University, Qingdao 266237, China

2. Southern Marine Science and Engineering Guangdong Laboratory (Zhuhai), Zhuhai 519082, China

3. Laboratory for Coastal Ocean Variation and Disaster Prediction, College of Ocean and Meteorology, Guangdong Ocean University, Zhanjiang 524088, China

4. Key Laboratory of Climate, Resources and Environment in Continental Shelf Sea and Deep Sea of Department of Education of Guangdong Province, Guangdong Ocean University, Zhanjiang 524088, China

5. National Marine Environmental Forecasting Center, Beijing 100086, China

6. Key Laboratory of Smart Earth, Beijing 100086, China

*zhangshouwen@sml-zhuhai.cn

Abstract

Storm surge is one of the most significant marine dynamic disasters affecting the coastal areas worldwide. A comprehensive study of its mechanisms is vital for improving forecasting capabilities and developing more prevention strategies. In this study, a two-dimensional (2D) numerical model based on the Advanced Circulation Model (ADCIRC) was employed to examine the characteristics of storm surges and the mechanisms of tide-surge interaction in the Pearl River Estuary (PRE) during Typhoon Nida (2016). Three distinct model runs were conducted to differentiate between variations in water levels attributable to astronomical tides, storm surges, and their combined effect. The results indicated that storm tide are primarily modulated by tides through tide-surge interactions. The nonlinear effect of tide-surge interaction is primarily generated by the nonlinear local acceleration term and convection term from the tide-surge interactions in the study area, as derived from the mathematical terms. However, in regions of shallow water, such as the northern part of Qi'ao Island and Shenzhen Bay, they are predominantly governed by the nonlinear wind stress term and bottom friction term. Furthermore, the variations in the y component of the nonlinear momentum terms are more significant than those in the x component. To investigate the impact of tidal phase on storm surge response to Typhoon Nida, the timing of landfall was altered in order to introduce variations in PRE characteristics. The results demonstrate that the contribution ratio of each nonlinear term remains relatively constant, while the magnitudes exhibit fluctuations contingent on the timing of landfall. However, further studies on additional typhoon events, especially with onshore winds, are needed, as well as a comprehensive consideration of the meteorological processes and the mechanisms of tidal-wave propagation inside and outside the estuary. The model system could still be improved in the future.

Keywords: Tide-surge interaction; Storm surge; ADCIRC; Nonlinear effect

1. Introduction

Storm surge are defined as an abnormal rise in sea level caused by atmospheric pressure and wind stress from phenomena such as tropical cyclones (TCs) and fronts. TCs, also known as typhoons or hurricanes, have the potential to induce storm surges with extreme water levels, which can resulting in significant economic losses and human casualties in coastal areas, particularly

43 when they coincide with high astronomical tides (Flather, 1994). The conventional method for
44 forecasting storm surges during TCs involves predicting the water level under a specified wind
45 field and then linearly add that water level to the predicted astronomical tides (Heaps, 1983).
46 However, numerous studies have demonstrated that the effect of tide-surge interaction is nonlinear
47 (Johns et al., 1985; Bernier and Thompson, 2007; Quinn et al., 2012). A comparison of
48 observations with the straightforward linear superposition of astronomical tides and individually
49 calculated storm surges indicates that discrepancies of up to 1-2 m (Rego and Li, 2010). During
50 periods of extreme water levels, nonlinear interactions occur within the estuarine area among tide,
51 storm surge, wave, and river streamflow (Hu et al., 2023). For instance, on beaches and barrier
52 islands, the contribution of wave runup to total water levels is significant and cannot be
53 overlooked (Vicens-Miquel et al., 2025).
54   The total water level can be divided into three main components: the astronomical tide, the
55 storm surge caused by atmospheric forcing, and the nonlinear residual level caused by tide-surge
56 interaction which represents a significant source of error in the prediction of storm surges (Idier et
57 al., 2012; Xu et al., 2016; Yang et al., 2019). Observations and simulations have indicated that
58 storm surges are influenced by astronomical tides, with the nonlinear effect of the tide-surge
59 interaction can significantly modulate water levels in shallow regions. There are two main
60 characteristics of storm surges due to the nonlinear effect of tide-surge interaction. One
61 characteristic is that the peak storm surge height near high tide is typically lower than that near
62 low tide, which could increase storm surge levels during the rising tide and decrease them at high
63 tide (Rossiter, 1961; Wolf, 1978; Horsburgh and Wilson, 2007; Olbert et al., 2013). Another
64 characteristic is the variation in storm surge intensity, where the storm surge is notably stronger
65 during low tide compared to high tide (Horsburgh and Wilson, 2007; Feng et al., 2016; Song et al.,
66 2020). The tide-surge interaction comprises three nonlinear physical processes: (a) the nonlinear
67 advective effect from the advective terms in the momentum equations; (b) the nonlinear bottom
68 friction effect with quadratic parameterisation; (c) the shallow water effect arising from the
69 nonlinear terms related to the total water depth in both the mass conservation equation and the
70 momentum equations (Zhang et al., 2010; Song et al., 2020; Zheng et al., 2020). Zhang et al.
71 (2010) found that bottom friction was the principal contributor to tide-surge interaction in the
72 Taiwan Strait. Rego and Li (2010) studied the storm surge induced by Hurricane Rita and revealed
73 that the advection terms were dominant over bottom friction with significant spatial-temporal
74 variations in the nonlinear terms. In strong current regions, the nonlinear advection term may also
75 play a key role in the dynamics of nonlinear tide-surge interactions (Wolf, 1978; Rego and Li,
76 2010; Yang et al., 2019; Hu et al., 2023). Valle - Levinson et al. (2013) found that Coriolis
77 accelerations and local accelerations due to alongshore current may significantly influence the
78 tidal modulation of storm surges.
79   The characteristics of storm surges and nonlinear effects in the Pearl River Estuary (PRE) are
80 especially complex, as its topography consists of deep channels, shallow shoals, and tidal flats.
81 This renders the PRE highly susceptible to storm surges induced by intense TCs (Zheng et al.,
82 2020). As a semi-enclosed bay, as shown in Fig 1c, Lingding Bay is regularly affected by both
83 storm surges and irregular semi-diurnal tides. The trumpet-shaped bay naturally funnels tidal
84 energy, leading to an amplification of tidal amplitude of at the top of the bay. However, specific
85 investigations concerning the variability of typhoon landfall timing to tide-surge interactions and
86 their impact on the temporal and spatial distribution of storm surges within the PRE are still scarce.
87 Due to the strong tidal dynamics and complex topography of the region, tide-surge interactions
88 along the PRE are significant, and the mechanisms are complex, which motivate this work.

Therefore, efficient and accurate marine forecasting, achieved through the analysis of mechanisms and precise modeling of storm surges induced by typhoons, are essential for mitigating typhoon-induced disasters in coastal regions.

The maximum storm surge induced by Typhoon Nida, which coincided with the astronomical high tide, resulted in severe economic losses, estimated at 112 million RMB. The principal objective of this study is to investigate the nonlinear residual levels associated with the tide-surge interactions caused by Typhoon Nida. Additionally, the objective is to investigate the dynamic mechanisms by establishing mathematical relationships between these nonlinear levels and the nonlinear dynamic terms. In this paper, a storm surge model for the PRE based on ADCIRC is utilized to investigate the mechanism of tide-surge interaction. In order to better characterize these impacts, different contributions to storm surge events can be calculated separately using the nonlinear terms of the two-dimensional theoretical momentum equations (Yang et al., 2019; Song et al., 2020; Hu et al., 2023).

In this paper, we will outline the characteristics of Typhoon Nida and provide a detailed description of the coupled tide-surge model, which is introduced and validated in Section 2. This is followed by an examination of the distribution of storm surge levels and nonlinear levels, along with a discussion of the results in Section 3. The conclusions derived from this study are detailed in Section 4.

2. Materials and Method

In this study, a coupled tide-surge model was built for Typhoon Nida. The typhoon and associated numerical model are introduced, and the model setup and validations are also described.

2.1 Typhoon Nida

Typhoon Nida was generated in the western North Pacific Ocean on 29 July 2016, and subsequently began to move westward rapidly. As shown in Fig 1a, Typhoon Nida classified as a sever tropical storm (STS), passed across the Philippines and entered the South China Sea (SCS) on July 31, 2016. It continued westward and made landfall as a typhoon (TY) at 19:30 on August 1 in Shenzhen, Guangdong Province, China. Nida had a central pressure of 970 hPa and maximum wind speed exceeding 42 m/s. After that, it weakened into a tropical storm (TS). At 0:00 on August 3, it further weakened into a tropical depression (TD) before dissipating. Notably, the peak water level increase induced by the storm surge of Typhoon Nida coincided with the highest high water (HHW) tidal phase.
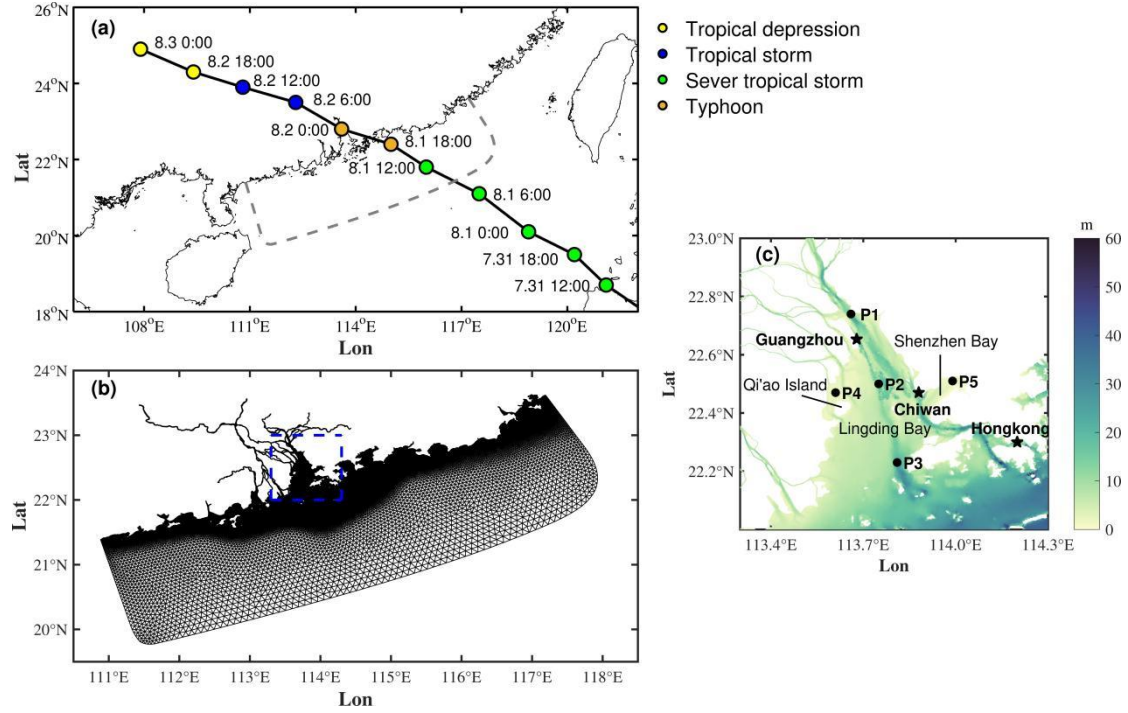
Figure 1. (a) The track and intensity of Typhoon Nida; (b) Model domain and grids of the study area; (c) Location and bathymetry of PRE. Stars represent the tidal gauges, and dots denote the calculation points of surge levels

2.2 The Numerical Model

The Advanced Circulation Model (ADCIRC) was used to simulate the tide and storm surge in PRE (Luettich et al., 1992). ADCIRC solves the primitive equations with the finite element method in space and with finite difference method in time (Westerink et al., 1992). Unstructured triangular grids were used in the horizontal plane to resolve dynamics in complex shorelines .

The basic vertically averaged governing equations, derived from momentum and continuity are as follows:

$$\frac{\partial H}{\partial t} + \frac{\partial}{\partial x}(UH) + \frac{\partial}{\partial y}(VH) = 0$$

$$\frac{\partial U}{\partial t} + U\frac{\partial}{\partial x}U + V\frac{\partial}{\partial y}U - fV = -g\frac{\partial(\zeta + P_s/g\rho_0)}{\partial x} + \frac{\tau_{sx} - \tau_{bx}}{H\rho_0} - \frac{D_x}{H} \tag{1}$$

$$\frac{\partial V}{\partial t} + U\frac{\partial}{\partial x}V + V\frac{\partial}{\partial y}V + fU = -g\frac{\partial(\zeta + P_s/g\rho_0)}{\partial y} + \frac{\tau_{sy} - \tau_{by}}{H\rho_0} - \frac{D_y}{H}$$

Where (U,V) are the x and y depth-averaged velocity components; $H=h+\zeta$ is the total water level; ζ is free surface elevation; h is the water depth; f is the Coriolis force parameter; g is gravitational acceleration; P_s is sea surface atmospheric pressure; ρ_0 is sea water density; (τ_{sx}, τ_{sy}) are the x and y components of surface wind stress; (τ_{bx}, τ_{by}) are the x and y components of bottom friction; (D_x, D_y) are the horizontal momentum diffusion terms.

The surface wind stress parameters (τ_{sx}, τ_{sy}) are computed as follows:

$$\tau_{sx} = \rho_a C_d W_x \sqrt{W_x^2 + W_y^2}, \tau_{sy} = \rho_a C_d W_y \sqrt{W_x^2 + W_y^2} \tag{2}$$

Where ρ_a is air density; (W_x, W_y) are the x and y components of wind speed. C_d is the wind drag coefficient, from Garratt (1977), it is calculated as follows:

143 $$C_d = 0.001 \times \left(0.75 + 0.067\sqrt{W_x^2 + W_y^2}\right) \tag{3}$$

144 The bottom friction (τ_{bx}, τ_{by}) is computed using the quadratic equation below:

145 $$\tau_{bx} = \rho_0 C_f U \sqrt{U^2 + V^2}, \tau_{by} = \rho_0 C_f V \sqrt{U^2 + V^2} \tag{4}$$

146 The bottom friction drag coefficient C_f is determined by model calibration.

147 The wind field model is crucial for accurate storm surge calculations. The analytical wind
148 model developed by Holland (1980) was applied in reconstruction of the wind field during
149 Typhoon Nida. The radial distribution of pressure and wind are determined as follows:

150 $$P_s(r) = P_c + (P_n - P_c) \cdot \left(-\frac{R_{max}}{r}\right)^B \tag{5}$$

151 $$W_g(r) = \sqrt{(P_n - P_c)\frac{B}{\rho_a}\left(\frac{R_{max}}{r}\right)^B \exp\left(-\frac{R_{max}}{r}\right)^B + \left(\frac{rf}{2}\right)^2} - \frac{rf}{2} \tag{6}$$

152 Where r is the distance from the typhoon center; P_n is the ambient pressure (1010 hPa) ; P_c is
153 the central pressure; R_{max} is the maximum wind radius and W_g is wind speed. The B parameter
154 determines the peak and intensity of the typhoon wind field, and is calculated as follows:

155 $$B = 1.5 + (980 - P_c)/120 \tag{7}$$

156 As B increases, the strong wind becomes increasingly localized near the radius of maximum
157 winds. For larger B, the wind drops off more abruptly both inside and outside the radius of
158 maximum wind. The R_{max} is calculated as follows:

159 $$R_{max} = 51.6\exp(-0.0223V_{max} + 0.0281\varphi) \tag{8}$$

160 V_{max} is the maximum wind and φ is latitude. The inflow angle caused by friction contributes
161 to wind field asymmetry, and a constant angle of 25 is used in this paper. The central pressure and
162 position data were retrieved from the China Meteorological Administration (CMA) tropical
163 cyclone database (Lu et al., 2021).
164

165 **2.3 Model setting**

166 The grid resolutions were set at a maximum of 600 m at the open boundaries, while the finest
167 resolution within the PRE region was 100 m. The domain space was discretized into 325582
168 triangular cells with 182048 nodes as shown in Fig 1b. The model utilized mean sea level as its
169 reference datum, and was forced at the open boundaries by 8 tidal constituents (including M_2, S_2,
170 N_2, K_2, K_1, O_1, P_1 and Q_1) derived from the global tidal model TPXO 9 (Egbert and Erofeeva,
171 2002). The typhoon wind field was generated using the wind model of Holland (1980). We used a
172 two-dimensional (2D) hydrodynamic model based on ADCIRC for the simulation runs. The
173 vertical current shear in well-mixed environment at shallow water depth is relatively small,
174 therefore, the 2D depth averaged model is sufficient to revel the physical processes of tide-surge
175 interaction (Idier et al., 2012; Zhang et al., 2017; Song et al., 2020). The model was run with a
176 cold start, setting both the current and water levels to zero at the initial time. The effect of river
177 flow and wind-generated waves were not considered in our model simulation, as the research is
178 primarily focused on the tide-surge interactions.

179 To verify the influence of the tide on storm surges, three simulations were conducted. One
180 was used to obtain the storm surge elevation (ζ_S) by only adding atmospheric forcing, another was
181 used to obtain the tide elevation (ζ_T) by only adding astronomical tidal forcing, and the other was
182 used to calculate the storm tide elevation (ζ_{TS}) by both atmospheric and tidal forcing. The storm
183 tide elevation (ζ_{TS}) can be written as the sum of the tide elevation (ζ_T), storm surge elevation (ζ_S),

184 and the nonlinear residuals (ζ_{Non}) due to tide-surge interaction, such that $\zeta_{TS} = \zeta_T + \zeta_S + \zeta_{Non}$.
185 Additionally, practical storm surge elevation $\zeta_{PS} = \zeta_{TS} - \zeta_T$ also considered in this paper.
186

3. Result

3.1 Tide and storm tide validation

189 The correlation coefficient (R), root mean square error ($RMSE$), model skill ($Skill$) were used
190 to validate the computed water level. The definition of the $Skill$ is determined as follows:

$$Skill = 1 - \frac{\sum_{n=1}^{N} |M_n - C_n|^2}{\sum_{n=1}^{N} \left(|M_n - \overline{M_n}|^2 + |C_n - \overline{M_n}|^2 \right)} \tag{9}$$

192 Where M_n and C_n are the measurements and model computed results, respectively, at N
193 discrete point.
194 The computed astronomical tides were initially assessed at three hydrological stations,
195 Chiwan, Hong Kong, and Guangzhou, over the period from July 2 to July 30, 2016, as shown in
196 Fig 2. The simulation results demonstrated a close match with the measurements obtained at these
197 three hydrological stations, as detailed in Table 1. The model predictions exhibited an excellent
198 agreement with the reconstructed astronomical tide, with $RMSE$ values at all three stations are <
199 0.27 m. Additionally, both the R values and $Skill$ values are generally above 0.91.
200

201 **Table 1.** Comparisons of tide and storm tide between the model simulations and observations

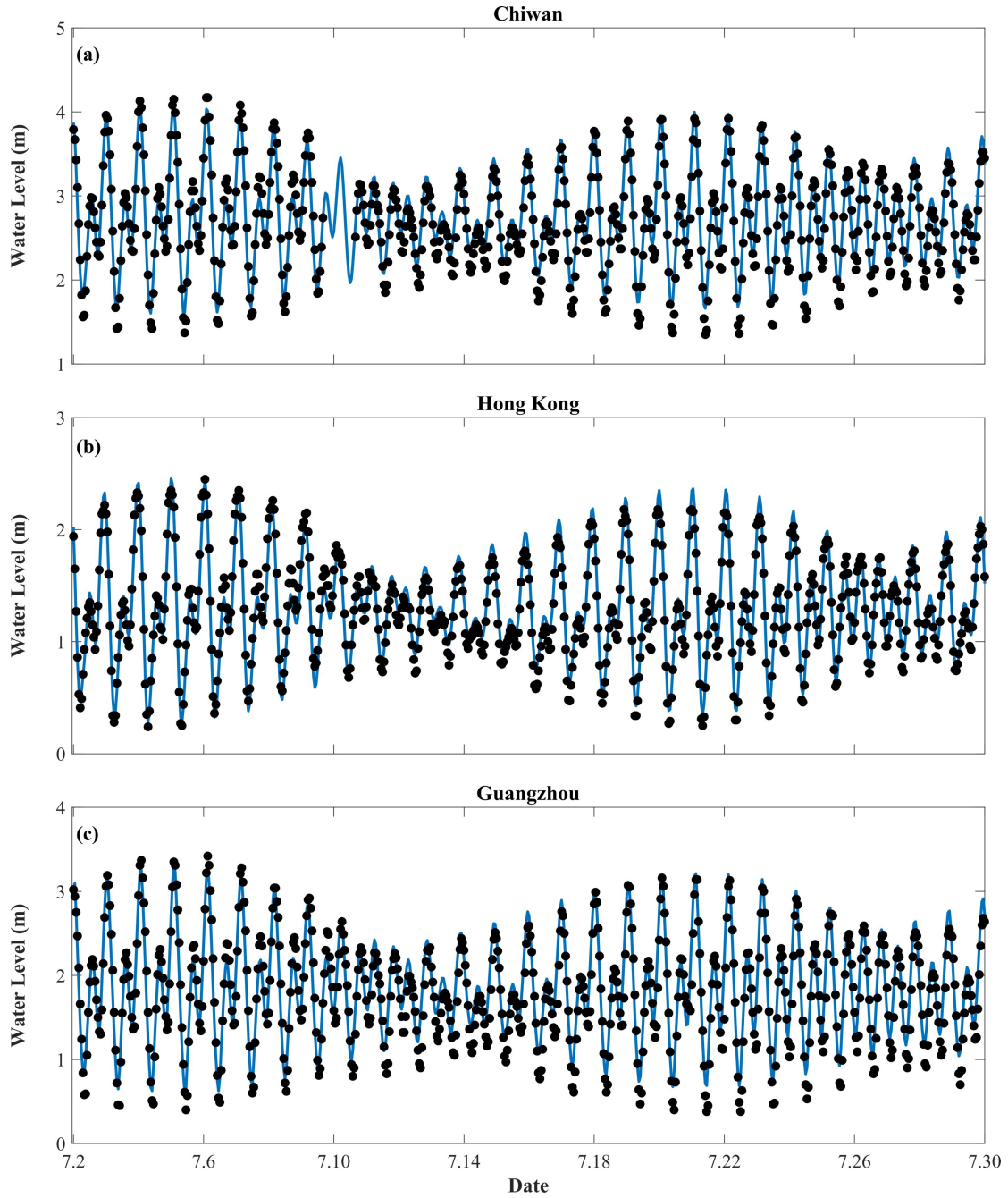|	Station	Chiwan	Hong Kong	Guangzhou
Tide	R	0.9470	0.9749	0.9206
	RMSE (m)	0.2046	0.1047	0.2629
	Skill	0.9368	0.9745	0.9112
Storm tide	R	0.9023	0.9728	0.8959
	RMSE (m)	0.3144	0.2503	0.3467
	Skill	0.8912	0.9169	0.8874

202

Figure 2. Time series comparisons of measured and modeled astronomical tide levels at (a) Chiwan gauge (b) Hong Kong gauge (c) Guangzhou gauge

The model simulated storm tide levels were further compared with the observed total water levels at the aforementioned three stations, as depicted in Fig 3. At all three stations mentioned above, the recorded water level reached its maximum (exceeding 2 m) on the evening of August 1, shortly after Typhoon Nida made landfall. At the Chiwan station, the water level exceeded 4 m, with a positive extreme value error of 0.21 m between the simulated and measured data. At the Hong Kong station, there was 0.13 m error of the positive extreme value between the simulated data and the measured. Similarly, at the Guangzhou station, the positive extreme value error between the model simulated storm tide and the measured data was 0.33 m. As illustrated in Table 1, the *R* value, *RMSE* value and the *Skill* value demonstrate that the simulation is functioning effectively.

7

217　　　The numerical results shows that when Nida approached to the PRE, the simulation of
218　increased water was underestimated, resulting in significant errors in storm tide prediction.
219　However, the simulated results for maximum water levels are in close alignment with the observed
220　values, thereby demonstrating that the model employed in this study is an effectively
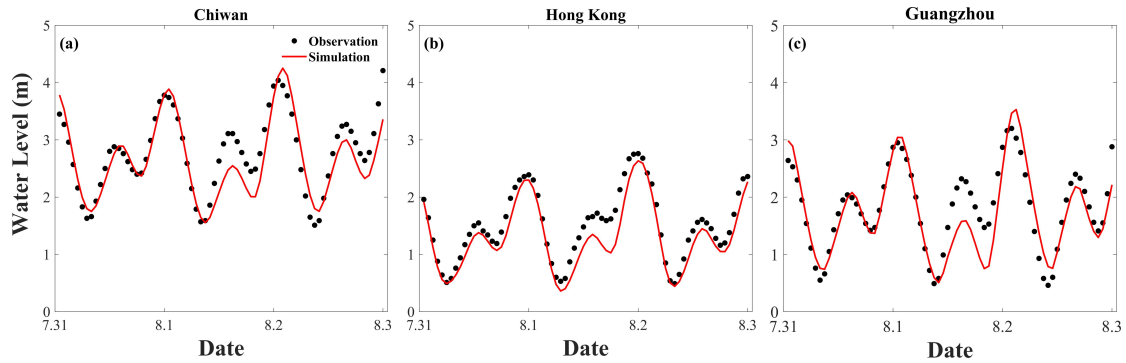221　representation of the tidal-surge interactions within the study area.
222

223
224　**Figure 3.** Time series comparisons of measured and modeled storm tide levels at (a) Chiwan gauge (b)
225　Hong Kong gauge (c) Guangzhou gauge
226

3.2 Storm surge characteristics of Typhoon Nida

228　　　Typhoon Nida passed through the PRE during a spring tide, coinciding with the maximum
229　storm surge at the HHW tidal phase. Based on this phenomenon, five tidal phases were selected
230　for investigate the evolution of storm surges before or after Typhoon Nida made landfall. The
231　spatial and temporal distribution characteristics of storm tides elevation during various tidal
232　phases in the PRE are illustrated in Fig 4. Five points were selected for examination within the
233　internal (P1), middle (P2), external (P3), northern part of Qi'ao Island (P4), and Shenzhen Bay (P5)
234　regions of the PRE, as shown in Fig 1c. Notably, the water depth at points P1, P2, and P3 exceeds
235　10 m, while the water depth at points P4 and P5 is less than 10 m. At 9:00 on 1 August, during the
236　lowest low water (LLW) tidal phase, the PRE area showed a decrease in water level which was
237　affected by the tide (Fig 4a). The offshore wind exhibited a tendency to decrease the water level.
238　While the nonlinear residuals were positive in Shenzhen Bay and the northern part of Qi'ao Island
239　(Fig 4b). At 15:00 on 1 August, which coincides with the lowest high water (LHW) tidal phase,
240　the total water elevation in PRE exhibited a negative to positive trend from northeast to southwest,
241　the offshore wind make some contribution. The most notable decline in water level is observed in
242　Shenzhen Bay (Fig 4d). At the same time, the nonlinear residuals are negative throughout
243　Lingding Bay, with the exception of its upper region (Fig 4e). At 19:00 on 1 August, during the
244　highest low water (HLW) tidal phase, both offshore wind and tide conditions resulted in a negative
245　trend in the elevation of storm tide in the PRE area, with the most significant negative values
246　occurring from northeast to southwest. Notably, the most substantial decrease in water level was
247　observed in Shenzhen Bay (Fig 4g). While the nonlinear residuals are positive, their impact is
248　particularly significant in Shenzhen Bay and the northern part of Qi'ao Island (Fig 4h). During the
249　HHW tidal phase, the storm tide elevation in the PRE area exhibits a most substantial increase
250　(Fig 4j). Conversely, during the same phase, the nonlinear residual levels exhibit a most significant
251　decrease (Fig 4k). Furthermore, at 10:00 on 2 August, during the LLW tidal phase, the storm tide
252　elevation in the PRE area was negative which was predominantly attributed to the tide. The
253　onshore wind exhibited a negligible effect on the water level, while the nonlinear residuals were
254　positive.

A comprehensive time series of storm surge elevation (ζ_S), tide elevation (ζ_T), storm tide elevation (ζ_{TS}), practical storm surge elevation (ζ_{PS}) and nonlinear residuals (ζ_{Non}) for each of the five points in the study area are presented in Fig 4. The positive storm surge elevation at three points (P1, P2, and P3) exhibited a notable increase from the outer to the inner regions of Lingding Bay. When Typhoon Nida made landfall, the nonlinear residuals reached their positive extreme value and subsequently reached their negative extreme value before the water elevation experienced its most substantial increase. The nonlinear residuals of P1, P2 and P3 reached their positive extremes of 0.19 m, 0.14 m and 0.04 m, respectively. This resulted in the induction of effects associated with the falling tide. The nonlinear residuals exhibited a decrease after Typhoon Nida made landfall and reached their negative extremes near the time of the positive extremes in storm surge elevation. Specifically, the negative extreme values of the nonlinear residuals at P1, P2 and P3 were -0.43 m, -0.29 m and -0.11 m, respectively. The nonlinear effect within the PRE exhibited a notable increase from the exterior towards the interior. Additionally, the positive extreme values of nonlinear residuals for P4 and P5 were 0.16 m and 0.14 m, respectively. While the negative extreme values of nonlinear residuals for P4 and P5 were both -0.29 m each. These findings indicate that the overall impact of Typhoon Nida was characterized by a greater decrease in nonlinear residuals than any increase.

The primarily concern is the increase in water level, which exerts the most significant influence on the elevation of the storm tide. The contributions of the storm surge elevation, the tide elevation, the practical surge elevation, and the nonlinear residuals to the storm tide elevation are calculated from five points in the PRE region, as illustrated in Table 2. It is evident from our findings that both storm surge and the tide make positive contributions to the elevation of storm tide. In contrast, the nonlinear residuals have been demonstrated to exert a negative influence on storm tide elevation. The practical surge contribution at P1 is identified as the most significant among the five points. Especially, the nonlinear effect at P2 is the most pronounced when compared to the other points.
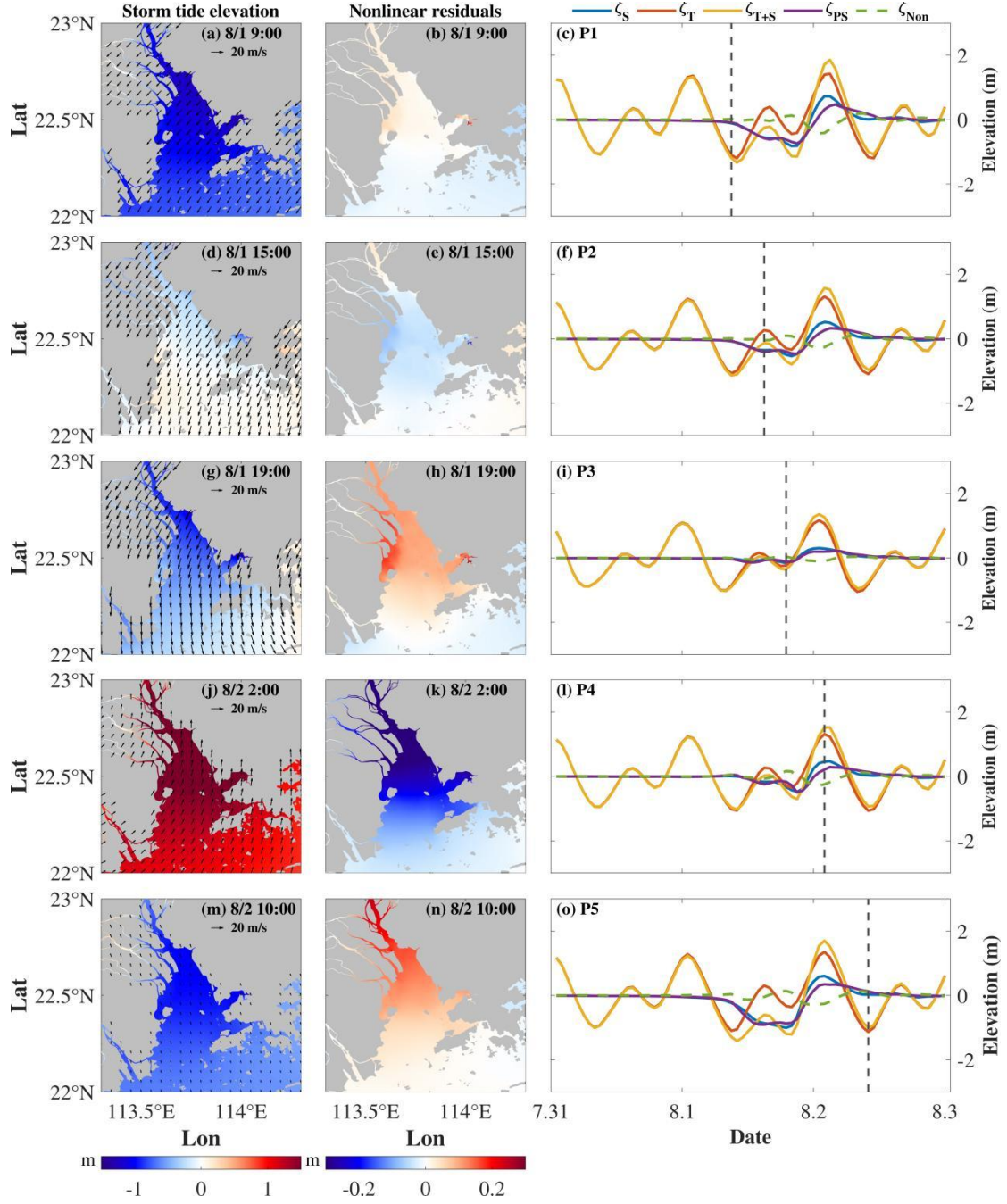
Figure 4. Storm tide elevation and wind vector (left), nonlinear residuals (middle) at different tidal phase and time series of water elevations (right) for P1, P2, P3, P4 and P5 locations; The dashed line indicates the time corresponding to the time on the left and middle graphs.

In order to emphasize the importance of the nonlinear effect, the ratio of the nonlinear residuals to the storm surge was calculated and compared with the ratio of the nonlinear residuals to the practical storm surge, as illustrated in Table 3. The ratio of the nonlinear residuals to the storm surge represents the extent to which the nonlinear effect amplifies or diminishes the direct impact of the storm surge. Meanwhile, the ratio of the nonlinear residuals to the practical storm surge provides insight into the extent to which the nonlinear effect contributes to the practical storm surge. It is observed that, among all five points, the influence of storm surges on water elevation is relatively minor at P3 due to nonlinear effects. Nevertheless, the effects in question have an almost 57% negative impact on practical storm surges. Notably, at P2, there is a markedly

negative contribution from nonlinear effects amounting to nearly 98%. This suggests that, in comparison to other points, P2 is subject to a more pronounced influence from storm surges, which can be considered to be a form of practical storm surges.

Table 2. The contribution to the storm tide elevation at the maximum moment of storm tide

Stations	Storm surge (%)	Tide (%)	Practical storm surge (%)	Nonlinear effect (%)
P1	39.17	76.87	23.13	-16.05
P2	33.05	83.35	16.65	-16.40
P3	22.36	85.80	14.20	-8.16
P4	30.79	80.82	19.18	-11.61
P5	35.72	79.61	20.39	-15.33

Table 3. The contribution of the nonlinear effect to the storm surge and practical storm surge

Stations	ζ_{Non} / ζ_{S} (%)	ζ_{Non} / ζ_{PS} (%)
P1	-40.97	-69.38
P2	-49.61	-98.47
P3	-36.49	-57.46
P4	-37.71	-60.54
P5	-42.91	-75.17

3.3 The characteristics of storm surge by different typhoon landfall time

The primary factors contributing to tide-surge interactions are the alteration of tidal phase caused by storm surges and the modulation of storm surges due to tides (Feng et al., 2019; Zheng et al., 2020). Accordingly, the typhoon landfall times were modified in order to examine the characteristics of storm surges occurring during different tidal phases. The nonlinear effects are subject to variation when typhoons make landfall at different tidal phases (Pandey and Rao, 2019). As shown in Fig 5, the practical storm surge at P1 shows minimal changes with different typhoon landfall times. When the positive increase in water elevation caused by storm surge coincides with the HHW tidal phase, the positive extreme values are smallest at each of the five points. The nonlinear residuals exhibited a decreases in both positive and negative extreme values from the inner to the outer regions of Lingding Bay. However, when the positive increase in water elevation due to storm surge coincides with HLW tidal phase, which is equivalent to an advance in landfall time by 6 h, it results in a significantly greater positive extreme value of the practical surge elevation compared to others, as shown in Table 4. The influence of tides on storm tide elevation is more pronounced than that of storm surges, while the nonlinear effect exhibits a negative contribution (see Table 5). When a positive increase in water elevation resulting from a storm surge coincides with the LHW tidal phase, corresponding to an 11 h advance in landfall time, the positive extreme value of the practical storm surge shows minimal variation compared to when it coincides with the HHW tidal phase. It has been demonstrated that both surges and tides have a positive effect on storm tide elevation. However, the increase in water level due to the storm surge is greater than that due to the tide. Consequently, the nonlinear effect shows a negative contribution resulting in a reduction in water level (see Table 6). When the positive increase in water elevation from a storm surge coincides with LLW tidal phase, occurring at the landfall time of Typhoon Nida advanced by 16 h, the contribution of practical storm surge to the storm tide elevation is negative. Meanwhile, the contributions from the nonlinear effect are positive (see
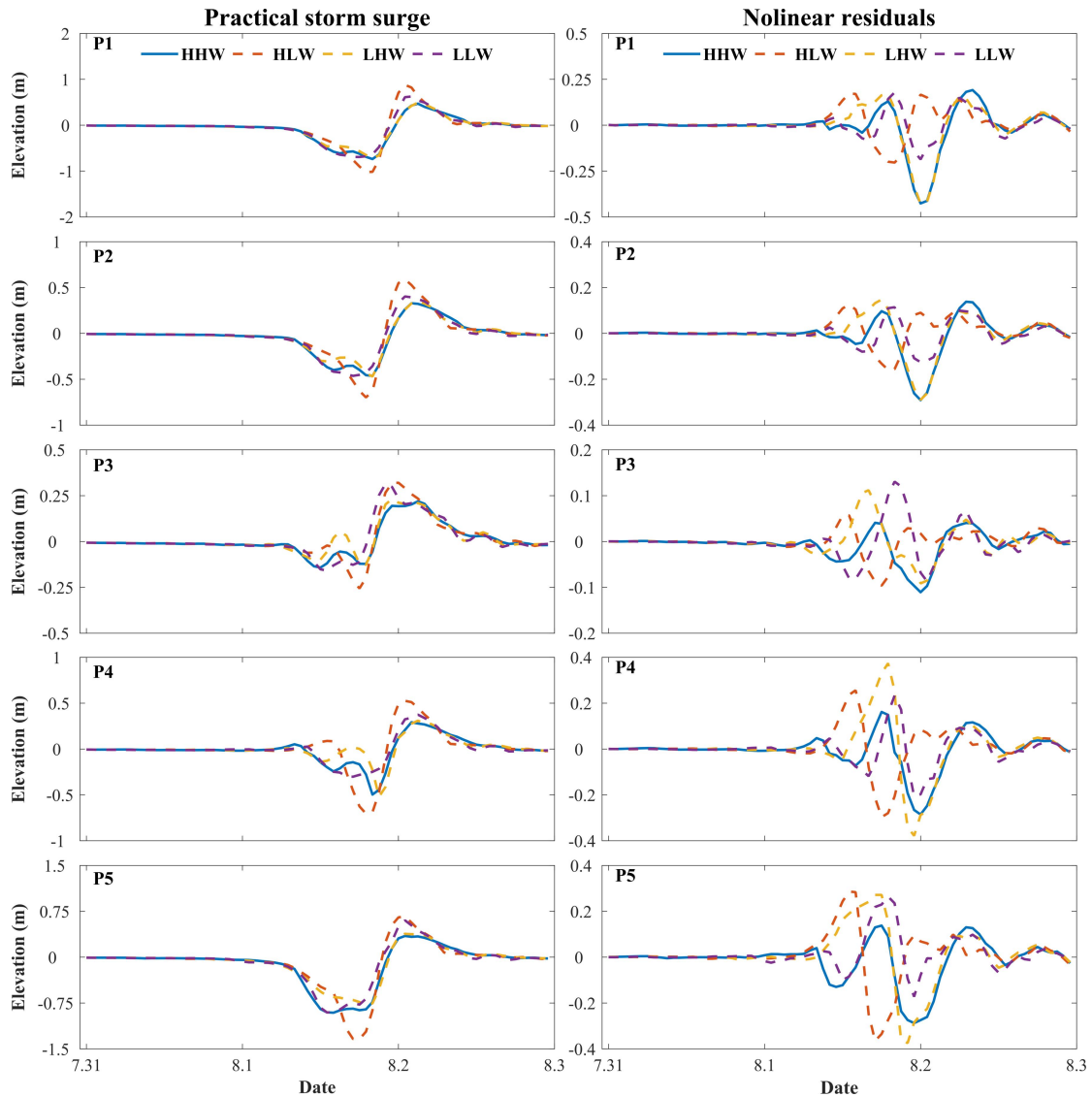
330

Figure 5. Time series of practical storm surge elevation (left) and nonlinear residuals (right) induced by different landfall time forcing at P1, P2, P3, P4 and P5

Table 4. Extreme value of practical storm surge elevation caused by different landfall time forcing at P1, P2, P3, P4 and P5

Stations	Negative extreme value of practical storm surge elevation（m）				Positive extreme value of practical storm surge elevation（m）			
	HHW	HLW	LHW	LLW	HHW	HLW	LHW	LLW
P1	-0.74	**-1.02**	-0.72	-0.63	0.47	**0.88**	0.49	0.63
P2	-0.46	**-0.70**	-0.47	-0.46	0.33	**0.59**	0.35	0.40
P3	-0.14	**-0.26**	-0.13	-0.16	0.22	**0.32**	0.23	0.31
P4	-0.50	**-0.70**	-0.52	-0.30	0.29	**0.53**	0.31	0.37
P5	-0.91	**-1.34**	-0.79	-0.90	0.35	**0.67**	0.38	0.60

Table 5. Contribution of the practical storm surge and nonlinear effect to storm tide elevation caused by different landfall time forcing at P1, P2, P3, P4 and P5

Stations	Practical storm surge（%）				Nonlinear effect（%）			
	HHW	HLW	LHW	LLW	HHW	HLW	LHW	LLW
P1	23.13	**193.17**	51.47	-174.92	-16.05	22.20	**-36.87**	27.84
P2	16.65	**224.68**	49.68	-68.08	-16.40	25.94	**-50.12**	20.09
P3	14.20	**354.88**	57.33	-36.91	-8.16	19.24	**-24.73**	10.67
P4	19.18	**172.11**	51.23	-67.90	-11.61	14.37	**-35.65**	25.29
P5	20.39	**207.21**	55.94	-133.17	-15.33	18.79	**-32.97**	1.06

Table 6. Extreme value of nonlinear residuals caused by different landfall time forcing at P1, P2, P3, P4 and P5

Stations	Negative extreme value of nonlinear elevation（m）				Positive extreme value of nonlinear elevation（m）			
	HHW	HLW	LHW	LLW	HHW	HLW	LHW	LLW
P1	-0.43	-0.20	-0.43	-0.19	0.19	0.17	0.17	0.18
P2	-0.29	-0.16	-0.29	-0.13	0.14	0.13	0.15	0.11
P3	-0.11	-0.10	-0.09	-0.09	0.04	0.06	0.11	0.13
P4	-0.29	-0.3	-0.38	-0.21	0.16	0.26	0.37	0.23
P5	-0.29	-0.36	-0.37	-0.17	0.14	0.29	0.27	0.26

Table 7. Contribution of the nonlinear effect to storm surge and practical storm surge caused by different landfall time forcing at P1, P2, P3, P4 and P5

Stations	ζ_{Non} / ζ_{S} (%)				ζ_{Non} / ζ_{PS} (%)			
	HHW	HLW	LHW	LLW	HHW	HLW	LHW	LLW
P1	-40.96	12.98	-41.74	-13.73	-69.38	11.49	-71.63	-15.92
P2	-49.61	13.05	-50.22	-22.78	-98.47	11.55	-100.89	-29.51
P3	-36.49	5.73	-30.14	-22.43	-57.46	5.42	-43.14	-28.91
P4	-37.71	9.11	-41.03	-27.14	-60.54	8.35	-69.59	-37.25
P5	-42.91	9.97	-37.08	-0.79	-75.17	9.07	-58.94	-0.80

Above all, the practical storm surge elevation and the nonlinear residuals are significantly modulated by tidal forces, particularly in areas of shallow water (Zhang et al., 2017; Zhang et al., 2019; Zhang et al., 2021). The practical storm surge exerts the greatest contribution to the storm tide elevation when the maximum of the storm surge coincides with the HLW tidal phase, as opposed to other phases. The nonlinear effect is negative during high tides (HHW and LHW) and positive during low tides (HLW and LLW) (Horsburgh and Wilson, 2007). The tidal contribution to the storm tide exceeds the surge contribution when the maximum of storm surges coincides with high tides. Conversely, the contribution of tides is less pronounced than that of the storm surge when the maximum of storm surges coincides with low tides. Notably, when the maximum of storm surges coincides with the LHW tidal phase, the contribution of the nonlinear effect is the greatest compared to other tidal phases (see Table 5). When the landfall time coincides with different tidal phases, the positive extreme value of nonlinear residuals changes little, whereas the negative extreme value of negative nonlinear residuals changes significantly as demonstrated in Table 6. As shown in Table 5, the practical storm surge makes the greatest contribution when the maximum of the storm surge coincides with the LHW tidal phase, compared to other tidal phases. The nonlinear effect has the greatest impact when the maximum of the storm surge coincides with

the HLW tidal phase. A comparison of the ratios reveals that both the ratio of nonlinear residuals to the storm surge and the ratio of nonlinear residuals to the practical storm surge are positive when their maximum coincides with the HLW tidal phase. Conversely, they are negative during other tidal phases (see Table 7). This indicates that an increase in water elevation due to nonlinear effects becomes significant only when the maximum of storm surge coincides with the HLW tidal phase.

3.4 Dynamic mechanism of nonlinear residual levels caused by Typhoon Nida

To further analyze the source of the tide-surge interaction and its nonlinear effects, we utilized the formula proposed by (Yang et al., 2019) for calculating these nonlinear terms. As shown in Fig 2, five representative points were selected to illustrate the nonlinear effects of tide-surge interactions in the PRE.

$$\frac{\partial U_{NS}}{\partial t} + \psi_x\left(U_{NS}, V_{NS}\right) - fV_{NS} - \tau_x^S - \tau_x^B = -g\frac{\partial \zeta_I}{\partial x}$$
$$\frac{\partial V_{NS}}{\partial t} + \psi_y\left(U_{NS}, V_{NS}\right) + fU_{NS} - \tau_y^S - \tau_y^B = -g\frac{\partial \zeta_I}{\partial y} \tag{10}$$

The calculated results of nonlinear dynamic terms, including the nonlinear local acceleration term $\frac{\partial U_{NS}}{\partial t}$ and $\frac{\partial V_{NS}}{\partial t}$, the nonlinear convection term ψ_x, ψ_y, the nonlinear Coriolis force term fU_{NS}, fV_{NS}, the nonlinear wind stress term τ_x^S, τ_y^S, and the nonlinear bottom friction term τ_x^B, τ_y^B at each points in x and y direction are shown in Fig 6:

In the eastward direction (x component) at P1, the nonlinear local acceleration term plays a dominant role, with some contribution from the nonlinear bottom friction term. It is important to note that this phenomenon occurs within Lingding Bay. It is concluded that the effects of nonlinear advection and Coriolis force are deemed negligible. As Typhoon Nida approached Lingding Bay after 18:00 on 1 August 2016, the local acceleration term exhibited an increase, reaching a positive extreme at 00:00 on 2 August 2016, which is similar to the Coriolis term. The advection term reached its positive extreme one hour later, occurring concurrently with the negative extreme of the nonlinear residuals. Although the wind stress term is minimal, the bottom friction term reached its negative extreme at 2:00 on 2 August 2016, coinciding with the storm surge reaching its positive extreme. In the northward direction (y component), the amplitude of nonlinear local acceleration remains large; however, it is surpassed by the leading role played by the nonlinear advection term which reached its positive extreme at 2:00 on 2 August 2016.

In the eastward direction at P2, the values of the various nonlinear terms were relatively small, contributing little to the overall nonlinear effect. With the wind stress term playing a minor role among all nonlinear terms. However, in the northward direction, the local acceleration term is the dominant factor. The value of this term reached its negative extreme at 22:00 on 1 August 2016, and reached its positive extreme at 6:00 on 2 August 2016.

In the eastward direction at P3, the nonlinear Coriolis term was the dominant factor, with values reaching their positive extreme at 23:00 on 1 August 2016. Concurrently, both the nonlinear advection term and the local acceleration term reached their positive extremes, with each term making a significant contribution. Among all the nonlinear terms, the wind stress plays a minor role.
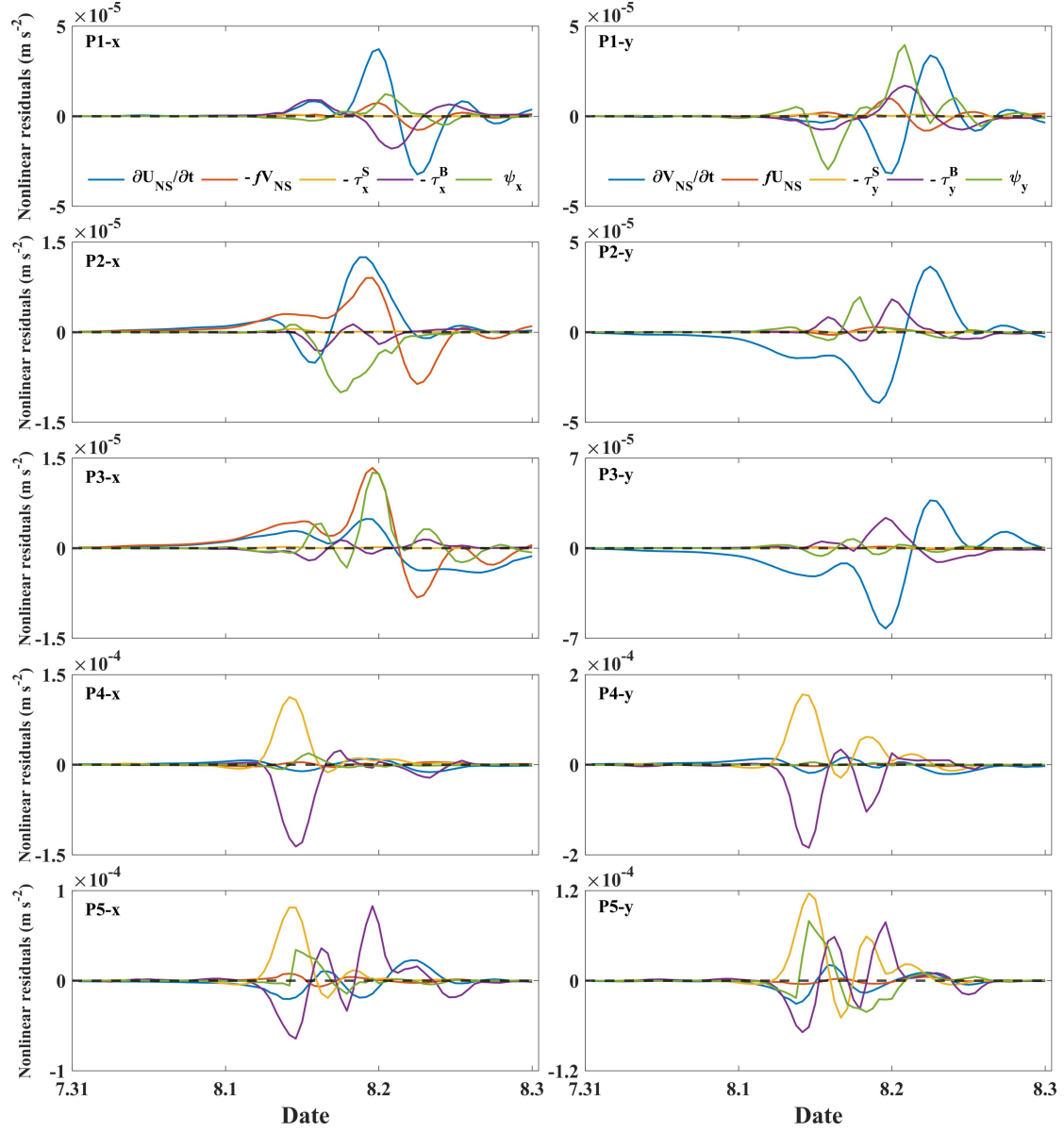
Figure 6. Time series of the nonlinear components of Typhoon Nida at P1, P2, P3, P4 and P5 in *x* direction (left) and *y* direction (right)

Given that P4 is situated in the northern part of Qi'ao Island and P5 in Shenzhen Bay, these two points represent areas of significant nonlinear effect of tide-surge interaction within the PRE region. As illustrated in Fig 6, in the eastward direction at P4, the nonlinear wind stress term plays a leading role and reached its positive extreme at 14:00 on 2 August 2016. It is also notable that the nonlinear bottom friction term plays a significant role. In the northward direction at P4, both the nonlinear wind stress and bottom friction terms contribute to the nonlinear effect. In the eastward direction at P5, the significance of the wind stress and bottom friction terms exceeds that of the other terms.

About all points, the results indicate that the gradient of the nonlinear residuals was stronger in the northerly direction than in the easterly direction (Hu et al., 2023), with the exception of the nonlinear Coriolis term. This study focuses on analyzing storm surges induced by Typhoon Nida using a two-dimensional (2D) model with high regulation unstructured grid, which enhances both accuracy and robustness of our conclusions. The establishment of direct mathematical

relationships between nonlinear residuals and dynamic terms through theoretical derivation provides valuable insights. It was found that the nonlinear acceleration term mainly contributes to the top of the bay, indicating a strong interaction between tidal current and storm-induced current (Song et al., 2020). Additionally, wind stress also affected the tide-surge interaction since the H was in the denominator of wind stress term, especially in shallow water area, such as the northern part of Qi'ao Island and Shenzhen Bay. Furthermore, it is noted that shallow water effects are more pronounced in Shenzhen Bay due to the restricted water depth over tidal flats (Zheng et al., 2020).

3.5 Dynamic mechanism of the nonlinear residuals influenced by different typhoon landfall time

To investigate the nonlinear momentum characteristics resulting from different tidal forcing, the nonlinear momentum terms were calculated. When the maximum increase in water elevation caused by storm surge coincides with the HLW tidal phase, the temporal changes of the nonlinear residuals are shown in Fig 7. In the eastward direction at P1, the dominant factor is the nonlinear local acceleration term, with a certain contribution from the nonlinear bottom friction term. Furthermore, the effects of nonlinear advection and Coriolis force also make significant contributions. In the northward direction, while the amplitude of the nonlinear local acceleration term remains considerable, it is surpassed by the influence of the nonlinear advection term. Both in the x component and the y component, the wind stress terms exhibit weak impact and can be neglected. In the eastward direction at P2, the values of various nonlinear terms were relatively small, with a negligible contribution to the nonlinear effect. Furthermore, the wind stress plays a minor role among all nonlinear terms. The nonlinear Coriolis term contributes to positive nonlinear residuals, whereas the advection term and the bottom friction term contribute negatively to nonlinear residuals. However, in the northward direction, the local acceleration term plays a leading role and reaches its negative extreme in nonlinear residuals at 16:00 on 1 August 2016. In the eastward direction at P3, the nonlinear Coriolis and nonlinear advection terms contribute to the dynamics. However, in the northward direction at P3, the dominant term is the nonlinear local acceleration term, with additional contributions from bottom friction and nonlinear advection terms. The wind stress plays a minor role among all nonlinear terms. In the eastward direction at P4, the nonlinear bottom friction term plays a dominant role, reaching its negative extreme at 18:00 on 1 August 2016. Following closely behind is the nonlinear wind stress term, which reached its positive extreme at 17:00 on 1 August 2016. In the northward direction at P4, both the nonlinear wind stress and bottom friction terms contribute to the nonlinear effect. Specifically, while the bottom friction term make a negative contribution to the nonlinear residuals, the wind stress contributes positively. The wind stress term reached its positive extreme at 17:00 on 1 August 2016, and the bottom friction term reached its negative extreme at the same time. In the eastward direction at P5, the wind stress and bottom friction terms are of greater significance than the other terms. In the northward direction at P5, the wind stress term and bottom friction term also exerted a dominant influence on the nonlinear residuals. Moreover, the absolute value of the positive extreme of the wind stress term is greater than that of the negative extreme of the bottom friction term. The advection term was so insignificant that it was recorded as negligible, resulting in a discontinuous time series.
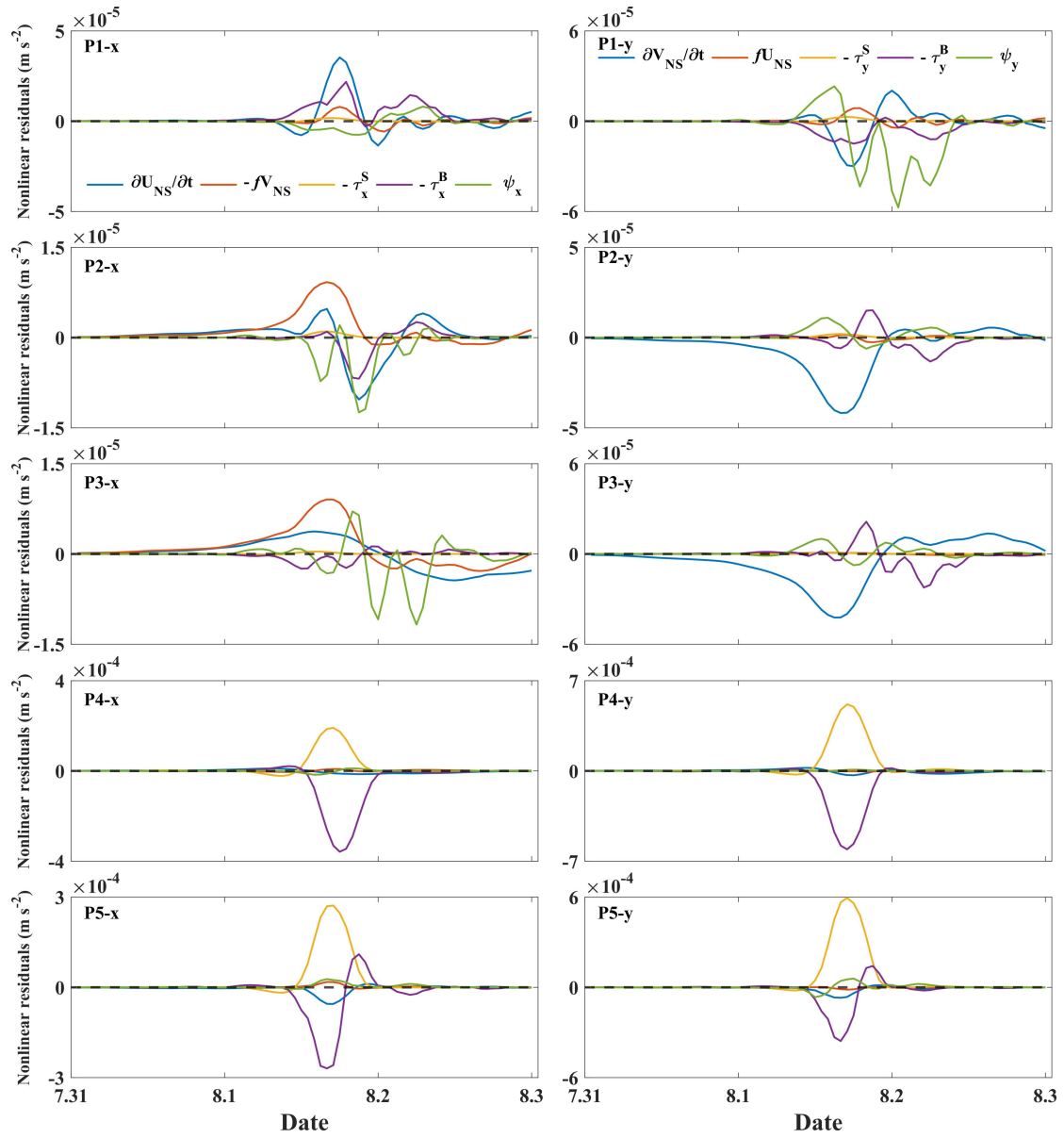
Figure 7. Time series of the nonlinear components at P1, P2, P3, P4 and P5 in *x* direction (left) and *y* direction (right) when maximum storm surge coincides with the HLW tidal phase
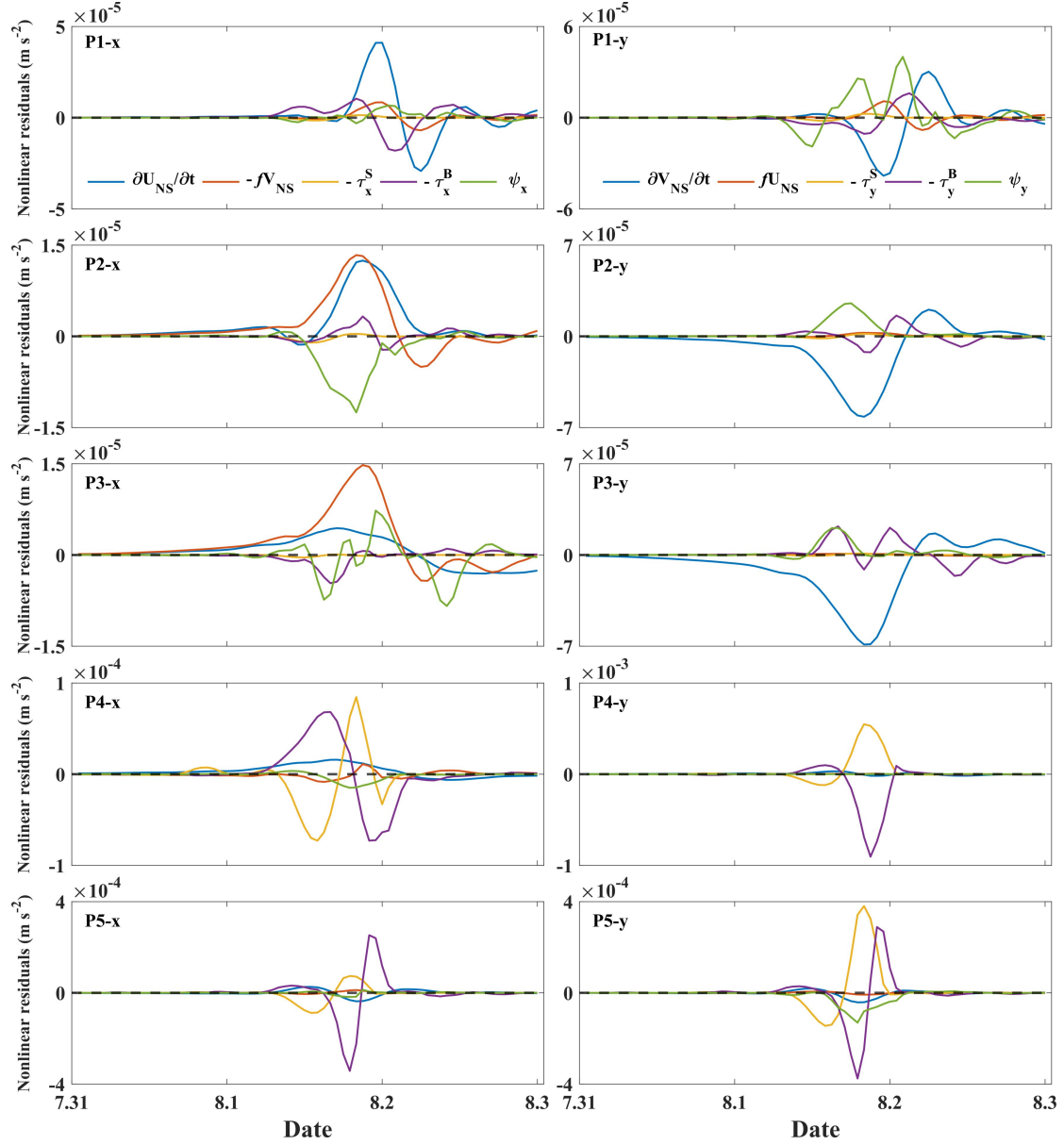
Figure 8. Time series of the nonlinear components at P1, P2, P3, P4 and P5 in *x* direction (left) and *y* direction (right) when the maximum storm surge coincides with the LHW tidal phase

When the maximum increase in water level caused by pure storm surge coincides with the LHW tidal phase, Figure 8 illustrates the time series changes of the nonlinear residuals. In the eastward direction at P1, the nonlinear local acceleration term is also the most significant contributor, followed by the nonlinear bottom friction term, which represents the second-largest contribution. Nonlinear advection and Coriolis force exert a considerable influence on the nonlinear residuals. In the northward direction, the nonlinear local acceleration term and the nonlinear advection term exert a major contributions. Both in the *x* component and *y* component, the wind stress term is weak and can be considered negligible. In the eastward direction at P2, both the bottom friction term and the wind stress term are significantly smaller compared to other terms. The positive nonlinear residuals are contributed by nonlinear local acceleration term while the negative ones are result of contributions from the nonlinear advection term and bottom friction term. However, in the northward direction at P2, it is observed that nonlinear local acceleration term plays a leading role, reaching its negative extreme value at 20:00 on 1 August 2016. In the

18

eastward direction at P3, the nonlinear Coriolis term exerts the greatest influence on the nonlinear residuals, while the nonlinear local acceleration term and the nonlinear advection term contribute substantially as well. However, in the northward direction at P3, the nonlinear local acceleration term is predominant, with the bottom friction term and the nonlinear advection term exerting influence. The wind stress and Coriolis effects are both minimal. In the eastward direction at P4, the nonlinear bottom friction term and the nonlinear wind stress term exert a greater impact than other terms. In the northward direction at P4, the nonlinear wind stress term and the bottom friction term significantly contribute to the nonlinear residuals. Notably, the absolute value of the extreme of the bottom friction term is greater than that of the wind stress term. The wind stress term reached its positive extreme at 20:00 on 1 August 2016, while the bottom friction term reached its negative extreme 1 h later. In the eastward direction at P5, the bottom friction term is the primary contributor, with the wind stress term providing a secondary contribution. In the northward direction at P5, the wind stress term and the bottom friction term exert a dominant influence on the nonlinear residuals, with the other terms having a negligible effect.
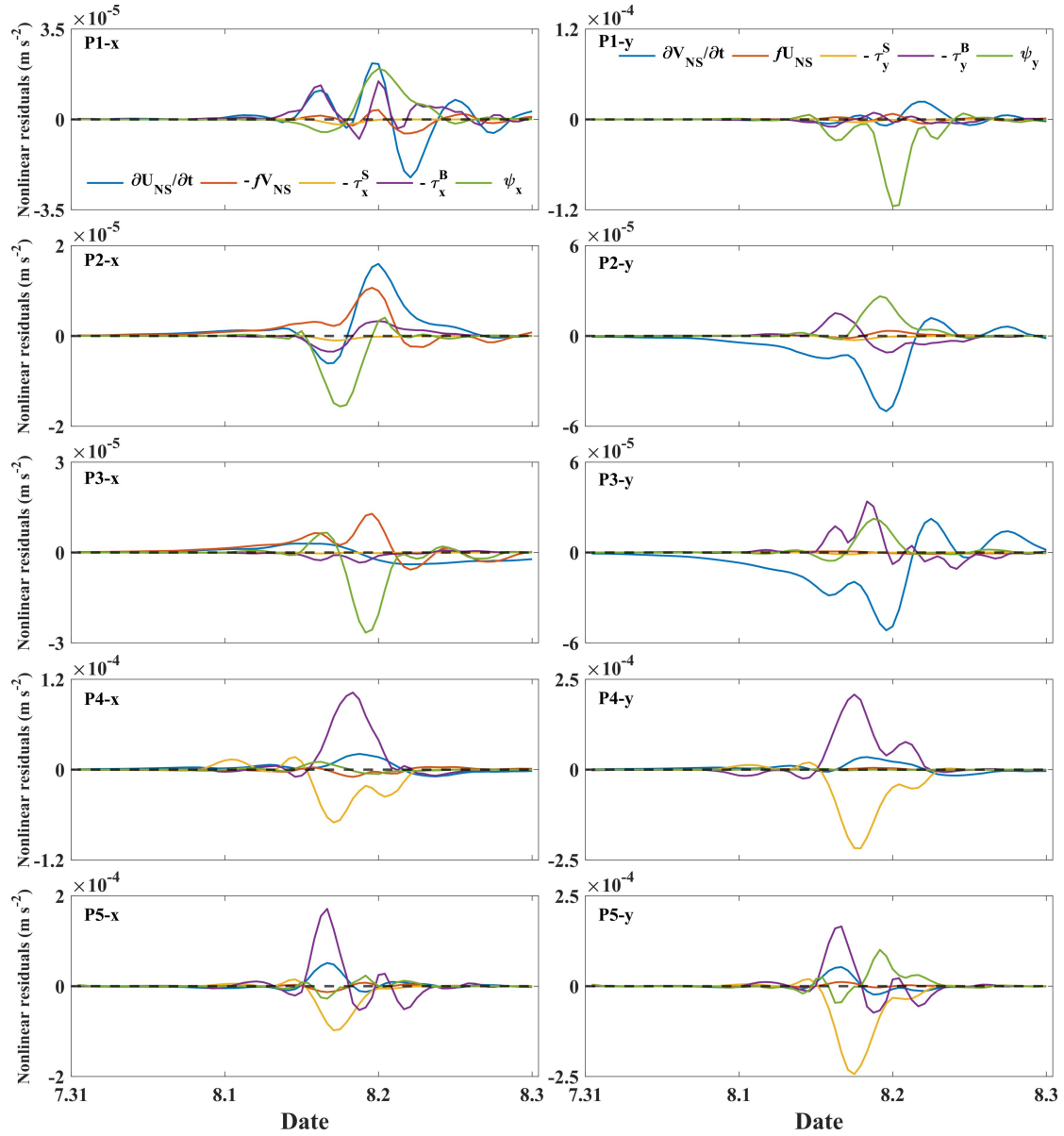

Figure 9. Time series of the nonlinear components at P1, P2, P3, P4 and P5 in *x* direction (left) and *y*

501   direction (right) when the maximum storm surge coincides with the LLW tidal phase.

502

503   When the maximum increase in water elevation caused by the storm surge coincides with the
504   LLW tidal phase, the time series changes of nonlinear residuals are shown in Fig 9. In the
505   eastward direction at P1, the nonlinear local acceleration term, the advection term and the bottom
506   friction term make major contributions. In the northward direction, the nonlinear advection term is
507   the most significant contributor. Both in x component and y component, the wind stress term is
508   relatively weak and can be considered negligible. In the eastward direction at P2, major
509   contributions are made by the nonlinear local acceleration term, the Coriolis term, and the
510   nonlinear advection term. However, in the northerly direction at P2, it is primarily influenced by
511   the local acceleration term which reaches its negative extreme in nonlinear residuals at 23:00 on 1
512   August 2016. Meanwhile, the advection term exerts a positive influence on the nonlinear residuals,
513   reaching its positive extreme at 22:00 on 1 August 2016. In the eastward direction at P3, the
514   nonlinear advection term exerts the dominant influence, with the nonlinear Coriolis term also
515   making a significant contributions. However, in the northward direction at P3, the nonlinear local
516   acceleration term is predominant, with the bottom friction and the nonlinear advection term also
517   contributing. The wind stress term and the Coriolis term are negligible in comparison. In the
518   eastward direction at P4, the nonlinear bottom friction term and the nonlinear wind stress term
519   make greater contributions than the other terms, with the nonlinear bottom friction term playing a
520   leading role and providing a positive contribution to the nonlinear residuals. In the northward
521   direction at P4, the nonlinear wind stress term and the bottom friction term make significant
522   contribution to the nonlinear effect. The positive contribution of the bottom friction nearly
523   balances the negative contribution of the wind stress. The wind stress reached its negative extreme
524   at 19:00 on 1 August 2016, while the bottom friction term reached its positive extreme 1 h earlier.
525   In the eastward direction at P5, the bottom friction term is the primary contributor, with the wind
526   stress term making the second largest contribution. In the northward direction at P5, the wind
527   stress term is the most significant contributor, with the other terms making comparatively less
528   impact.
529   The occurrence of storm surges in the estuary area is subject to influence of both typhoons
530   and tides. The interaction between these two forces on water levels has been demonstrated in
531   numerous studies. The elevation of storm surges in the PRE varies significantly depending on the
532   tidal phase during which they occur. A comparison of the nonlinear factors at those representative
533   points across different tidal phases can make a better understanding of the mechanisms underlying
534   the tide-surge interaction. The analysis of the nonlinear terms in the nonlinear residuals revealed
535   that when storm surges coincide with high tides (HHW and LHW), the nonlinear acceleration term
536   predominant affects the y component at P1. Conversely, when storm surges coincide with low
537   tides (HLW and LLW) at P1, the nonlinear advection term is the dominant factor. In the eastward
538   direction, the nonlinear acceleration term consistently plays a dominant role at P1. In the
539   northward direction, both P2 and P3 are characterized by a predominant influence of the nonlinear
540   acceleration term. In instances where storm surges occur concurrently with different tidal phases,
541   the proportionate contribution of each nonlinear term remains almost unchanged, but their
542   magnitudes vary. The results illustrate that the primary source of the tide-surge interaction
543   nonlinear effects within the PRE is the effect of the tide's velocity. While in shallow water area,
544   such as the northern part of Qi'ao Island and Shenzhen Bay, the tide-surge interaction nonlinear
545   effects are predominantly influenced by a combination of wind and bottom friction.

546

4. Conclusions

An ADCIRC model has been utilized to simulate the storm surges in the PRE induced by Typhoon Nida. Results from several numerical experiments investigating the interaction between tides and storm surges indicate that when the tidal effect is incorporated, the simulations agree well with observational data.

To study the characteristics of tide-surge interaction in the PRE, three types of model runs were conducted, from which the storm tide, the astronomical tide, the storm surge, the practical storm surge and the residual elevation due to the tide-surge interaction were obtained. The results show that, the storm surge is significantly modulated by the tide due to the tide-surge interaction. A direct mathematical relationship between nonlinear residuals and dynamic influencing factors has been established. This derivation includes the local acceleration term, the Coriolis force term, the wind stress term, the bottom friction term and the nonlinear advection term. The nonlinear momentum term can reflect the momentum response of different areas within the estuary to nonlinear effects. The momentum equation facilitates the establishment of a relationship between the nonlinear factors of tide-surge interactions and the underlying physical processes. A comparison of nonlinear factors at representative points from the inner to the outer bay has demonstrated that the local acceleration term and the nonlinear advection term exert a predominant influence on the nonlinear dynamics. However, in the case of Shenzhen Bay and the northern part of Qi'ao Island, it is the wind stress term and the bottom friction term that emerge as the dominant nonlinear factors.

To further investigate the relationship between tidal phases and storm surges, we adjusted the landfall time of Typhoon Nida in our model simulations. The results shows that both the practical storm surge level and the nonlinear level are significantly modulated by tidal forces, especially in shallow water areas. In instance where the maximum of storm surge coincides with a high tides, the contribution of the tide to the storm tide is greater than that of the storm surge. Conversely, the contribution of tides to the storm tide is less than that of the storm surge when the maximum of the storm surge coincides with low tides. The analysis revealed that the nonlinear effect of tide-surge interaction is positive when the maximum of storm surge coincides with low tidal phases (LLW and HLW). On the contrary, this nonlinear effect becomes negative when the maximum of the storm surge coincides with high tidal phases (HHW and LHW). Notably, when the maximum of storm surges coincides with the LHW tidal phase, the contribution of the nonlinear effect is the greatest in comparison to other tidal phases. The ratio of nonlinear residuals to the storm surge and the ratio of the nonlinear residuals to the practical storm surge are both positive when the maximum of the storm surge coincides with the HLW tidal phase, while the ratios during other tidal phases are negative.

Although similar results were also presented in other studies (Song et al., 2020; Hu et al., 2023), the discussions of nonlinear momentum for different tidal phases are still lacking. We calculated the nonlinear terms to discuss the characteristics and mechanisms of tide-surge interaction. When storm surges coincide with different tidal phases, the contribution ratio of each nonlinear term remains almost unchanged, but their magnitudes exhibit notable variation. The results illustrate that the primary source of the tide-surge interaction nonlinear effects within the PRE is the effect of the tide's velocity. In areas of shallow water, such as the northern part of Qi'ao Island and Shenzhen Bay, the tide-surge interaction nonlinear effects are predominantly influenced by a combination of wind and bottom friction.

Taking Typhoon Nida as a case study, the present research reveals the detailed characteristics

of tide-surge interaction in the PRE. The present results of this study can provide valuable information for understanding the tide-surge interaction mechanism and improving storm surges prediction within the PRE. However, further studies on additional typhoon events may be needed, along with a comprehensive consideration of meteorological processes and the mechanisms of tidal-wave propagation within and outside the estuary, and the model system could still be improved in the future.

Reference

Bernier, N. and Thompson, K.: Tide-surge interaction off the east coast of Canada and northeastern United States, J. Geophys. Res.-Oceans, 112, https://doi.org/10.1029/2006JC003793, 2007.

Egbert, G. D. and Erofeeva, S. Y.: Efficient inverse modeling of barotropic ocean tides, J. Atmos. Ocean. Technol., 19, 183-204, http://doi.org/10.1175/1520-0426(2002)019<0183:EIMOBO>2.0.CO;2, 2002.

Feng, J., Jiang, W., Li, D., Liu, Q., Wang, H., and Liu, K.: Characteristics of tide–surge interaction and its roles in the distribution of surge residuals along the coast of China, J. oceanogr., 75, 225-234, https://doi.org/10.1007/s10872-018-0495-8, 2019.

Feng, X., Olabarrieta, M., and Valle-Levinson, A.: Storm-induced semidiurnal perturbations to surges on the US Eastern Seaboard, Cont. Shelf. Res., 114, 54-71, https://doi.org/10.1016/j.csr.2015.12.006, 2016.

Flather, R.: Storm surge Prediction Model for the Northern Bay of Bengal with Application to Cyclone Disaster in April 1991, J. Phys. Oceanogr., https://doi.org/10.1175/1520-0485(1994)024<0172:ASSPMF>2.0.CO;2, 1994.

Garratt, J.: Review of drag coefficients over oceans and continents, Mon. Wea. Rev., 105, 915-929, https://doi.org/10.1175/1520-0493(1977)105<0915:RODCOO>2.0.CO;2, 1977.

637   Heaps, N.: Storm surges, 1967–1982, Geophy. J. Int., 74, 331-376,
638   https://doi.org/10.1111/j.1365-246X.1983.tb01883.x, 1983.
639   Holland, G. J.: An Analytic Model of the Wind and Pressure Profiles in Hurricanes, Mon. Wea. Rev.,
640   108, 1212-1218, https://doi.org/10.1175/1520-0493(1980)108<1212:AAMOTW>2.0.CO;2,
641   1980.
642   Horsburgh, K. and Wilson, C.: Tide-surge interaction and its role in the distribution of surge residuals
643   in the North Sea, J. Geophy. Res.-Oceans, 112, https://doi.org/10.1029/2006JC004033, 2007.
644   Hu, S., Liu, B., Hu, M., Yu, X., Deng, Z., Zeng, H., Zhang, M., and Li, D.: Quantification of the
645   nonlinear interaction among the tide, surge and river in Pearl River Estuary, Estuar., Coast
646   Shelf S., 290, 108415, https://doi.org/10.1016/j.ecss.2023.108415, 2023.
647   Idier, D., Dumas, F., and Muller, H.: Tide-surge interaction in the English Channel, Nat. Hazards Earth
648   Syst. Sci., 12, 3709-3718, https://doi.org/10.5194/nhess-12-3709-2012, 2012.
649   Johns, B., Rao, A., Dubinsky, Z., and Sinha, P.: Numerical modelling of tide-surge interaction in the
650   Bay of Bengal, Philosophical Transactions of the Royal Society of London. Series A,
651   Mathematical Physical Sciences, 313, 507-535, https://doi.org/10.1098/rsta.1985.0002, 1985.
652   Lu, X., Yu, H., Ying, M., Zhao, B., and Wan, R.: Western North Pacific Tropical Cyclone Database
653   Created by the China Meteorological Administration, Adv. Atmos. Sci., 38, 10,
654   https://doi.org/10.1007/s00376-020-0211-7, 2021.
655   Luettich, R. A., Westerink, J. J., and Scheffner, N. W.: ADCIRC: an advanced three-dimensional
656   circulation model for shelves, coasts, and estuaries. Report 1, Theory and methodology of
657   ADCIRC-2DD1 and ADCIRC-3DL, 1992.
658   Olbert, A. I., Nash, S., Cunnane, C., and Hartnett, M.: Tide–surge interactions and their effects on total
659   sea levels in Irish coastal waters, Ocean Dynamics, 63, 599-614,
660   https://doi.org/10.1007/s10236-013-0618-0, 2013.
661   Pandey, S. and Rao, A.: Impact of approach angle of an impinging cyclone on generation of storm
662   surges and its interaction with tides and wind waves, J. Geophys. Res.-Oceans, 124,
663   7643-7660, https://doi.org/10.1029/2019JC015433, 2019.
664   Quinn, N., Atkinson, P. M., and Wells, N. C.: Modelling of tide and surge elevations in the Solent and
665   surrounding waters: The importance of tide–surge interactions, Estuar., Coast. Shelf S., 112,
666   162-172, https://doi.org/10.1016/j.ecss.2012.07.011, 2012.
667   Rego, J. L. and Li, C.: Nonlinear terms in storm surge predictions: Effect of tide and shelf geometry
668   with case study from Hurricane Rita, J. Geophys. Res.-Oceans, 115,
669   https://doi.org/10.1029/2009JC005285, 2010.
670   Rossiter, J. R.: Interaction between tide and surge in the Thames, Geophys. J. Int., 6, 29-53,
671   https://doi.org/10.1111/j.1365-246x.1961.tb02960.x, 1961.
672   Song, H., Kuang, C., Gu, J., Zou, Q., Liang, H., Sun, X., and Ma, Z.: Nonlinear tide-surge-wave
673   interaction at a shallow coast with large scale sequential harbor constructions, Estuar., Coast
674   Shelf S., 233, 106543, https://doi.org/10.1016/j.ecss.2019.106543, 2020.
675   Valle-Levinson, A., Olabarrieta, M., and Valle, A.: Semidiurnal perturbations to the surge of Hurricane
676   Sandy, Geophys. Res. Lett., 40, 2211-2217, https://doi.org/10.1002/grl.50461, 2013.
677   Vicens-Miquel, M., Tissot, P. E., Colburn, K. F., Williams, D. D., Starek, M. J., Pilartes-Congo, J.,
678   Kastl, M., Stephenson, S., and Medrano, F. A.: Machine-Learning Predictions for Total Water
679   Levels on a Sandy Beach, J. Coast. Res., 41, 57-72,
680   https://doi.org/10.2112/JCOASTRES-D-24-00016.1, 2025.
681   Westerink, J. J., Blain, C. A., Luettich, R. A., and Scheffner, N. W.: ADCIRC: An Advanced
682   Three-dimensional Circulation Model for Shelves, Coasts and Estuaries, Report 2-User's

683   Manual for ADCIRC-2DDI, US Army Corps of Engineers Washington, DC1992.

684 Wolf, J.: Interaction of tide and surge in a semi-infinite uniform channel, with application to surge
685   propagation down the east coast of Britain, Applied Mathematical Modelling, 2, 245-253,
686   https://doi.org/10.1016/0307-904X(78)90017-3, 1978.

687 Xu, J., Zhang, Y., Cao, A., Liu, Q., and Lv, X.: Effects of tide-surge interactions on storm surges along
688   the coast of the Bohai Sea, Yellow Sea, and East China Sea, China Earth Sci., 59, 1308-1316,
689   https://doi.org/10.1007/s11430-015-5251-y, 2016.

690 Yang, W, Yin, B., Feng, X., Yang, D., Gao, G., and Chen, H.: The effect of nonlinear factors on
691   tide-surge interaction: A case study of Typhoon Rammasun in Tieshan Bay, China, Estuar.,
692   Coast Shelf S., 219, 420-428, https://doi.org/10.1016/j.ecss.2019.01.024, 2019.

693 Zhang, H., Cheng, W., Qiu, X., Feng, X., and Gong, W.: Tide-surge interaction along the east coast of
694   the Leizhou Peninsula, South China Sea, Cont. Shelf. Res., 142, 32-49,
695   https://doi.org/10.1016/j.csr.2017.05.015, 2017.

696 Zhang, W., Teng, L., Zhang, J., Xiong, M., and Yin, C.: Numerical study on effect of tidal phase on
697   storm surge in the South Yellow Sea, J. Ocean. Limnol., 37, 19,
698   https://doi.org/10.1007/s00343-019-8277-8, 2019.

699 Zhang, W. Z., Shi, F., Hong, H. S., Shang, S. P., and Kirby, J. T.: Tide-surge Interaction Intensified by
700   the Taiwan Strait, J. Geophy. Res.-Oceans, 115, https://doi.org/10.1029/2009JC005762, 2010.

701 Zhang, X., Chu, D., and Zhang, J.: Effects of nonlinear terms and topography in a storm surge model
702   along the southeastern coast of China: a case study of Typhoon Chan-hom, Nat. Hazards, 107,
703   551-574, https://doi.org/10.1007/s11069-021-04595-y, 2021.

704 Zheng, P., Li, M., Wang, C., Wolf, J., Chen, X., De Dominicis, M., Yao, P., and Hu, Z.: Tide-surge
705   interaction in the Pearl River Estuary: a case study of Typhoon Hato, Front. Mar. Sci., 7, 236,
706   https://doi.org/10.3389/fmars.2020.00236, 2020.